proceedings

MDPI

Proceedings

Highly Sensitive H_2S Sensing with Gold and Platinum Surface-Modified ZnO Nanowire ChemFETs †

Angelika Kaiser [1,*], Erick Torres Ceja [1], Florian Huber [1], Ulrich Herr [2] and Klaus Thonke [1]

[1] Institute of Quantum Matter/Semiconductor Physics Group, Ulm University, 89081 Ulm, Germany; erick.torres-ceja@uni-ulm.de (E.T.C.); florian.huber@alumni.uni-ulm.de (F.H.); klaus.thonke@uni-ulm.de (K.T.)

[2] Institute of Functional Nanosystems, Ulm University, 89081 Ulm, Germany; ulrich.herr@uni-ulm.de

* Correspondence: angelika.kaiser@uni-ulm.de; Tel.: +49-(0731)-50-26132

† Presented at the 1st International Electronic Conference on Biosensors, 2–17 November 2020; Available online: https://iecb2020.sciforum.net/

Published: 2 November 2020

Abstract: In this work, we investigate the catalytic effects of gold (Au) and platinum (Pt) nanoparticle layer deposition on highly sensitive zinc oxide (ZnO) nanowires (NWs) used for selective H_2S detection in the sub-ppm region. Optimum quality pristine ZnO NWs were grown by high temperature chemical vapor deposition (CVD) in the vapor liquid solid growth (VLS) mode on silicon with a thin Au layer acting as a growth catalyst. The surface of pristine ZnO NWs was modified by systematic magnetron sputtering of discontinuous Au and Pt layers of 0–5 nm thickness. Resistive gas sensors based on the gas sensing mechanism of a chemical field effect transistor (ChemFET) with open gate, which is formed by hundreds of parallel aligned pristine Au-modified or Pt-modified ZnO NWs, were measured toward H_2S diluted in dry nitrogen (N_2) or in dry synthetic air at room temperature. Gas sensing results showed a largely improved response due to the catalytic effects of metal deposition on the ZnO NW surface. Controlled application of ZnO NW growth under optimized conditions and metal catalyst deposition showed a clear response enhancement toward 1 ppm H_2S from the initial 20% achieved with pristine ZnO to over 5000% with ZnO NWs covered by 5 nm of Au, and, hence, significantly lower than the limit of detection.

Keywords: ZnO; H_2S; Au; Pt; catalyst; ChemFET; gas sensor; eNose

1. Introduction

Over the past decade, numerous publications have highlighted the medical role of hydrogen sulfide (H_2S) for therapeutic applications and early diagnostics [1,2], traced in medical breath analysis, e.g., with the "electronic nose" approach [3]. It was shown that abnormal endogenous H_2S concentration levels in exhaled breath samples can be linked to airway inflammation in asthma patients, and, hence, H_2S functions as a potent biomarker.

Expired human breath mainly consists of nitrogen, oxygen, and carbon dioxide, in addition to numerous volatile organic compounds (VOCs) and sulfides (such as H_2S) in the low ppt-ppb concentration range. Using ion-molecule reaction mass spectrometry, Milloning et al. successfully linked an exhaled trace amount of 1.9 ppb of H_2S to gastroesophageal cancer [4]. Zhang et al. studied eosinophilic asthma and paucigranulocytic asthma in 97 patients. In their studies, both chronic asthma types showed correlation to exhaled endogenous H_2S concentrations of 7.7 ppb and 11.1 ppb, respectively [5]. A fast and selective detection of such small concentrations is challenging. Here, standard sensing procedures often use mass spectrometry, gas chromatography, or infrared (IR) gas sensors [6–8]. Despite offering a reliable and selective detection technique, the instruments for these

sensing approaches are bulky and expensive [7]. Moreover, breath sample preparation and analysis rely on big volume samples or the conversion of H_2S before detection [9], which appears to be difficult when used for real medical breath detection with patients.

A less expensive and simple sensing approach is based on the cost-effective production and application of nano-scaled metal oxides [10], which are used for integrated chemiresistive gas sensor arrays of electronic nose (eNose) sensing systems. Here, a vast variety of metal oxides for H_2S detection were investigated, including WO_3 [11], CuO [12], SnO_2 [13], $\alpha - Fe_2O_3$ [14], and ZnO [15]. Wu et al. presented a gas sensor based on $\alpha - Fe_2O_3$ nano-ellipsoids synthesized through a hydrothermal method with reliable sensing response towards 1-400 ppm of H_2S and an excellent detection limit of 100 ppb at 350 °C [16]. A fast and significant response toward 50 ppb of H_2S at room temperature was achieved by Wang et al. with a gas sensor based on hydrothermal ZnO nanorods [17].

The fabrication of highly selective room temperature gas sensors with enhanced gas sensing mechanics often requires the combination of several metal oxides, additional doping, or metal oxide surface modification with catalytic noble metals such as Au and Pt [18,19]. Sharma et al. demonstrated how gold-modified ZnO nanoplates showed an enhanced response toward H_2S [20], and Zhou et al. reached a detection limit of even 25 ppb for H_2S detection with well-dispersed Pt nanoparticles on a complex ZnO structure [21]. These studies present a promising material platform for highly sensitive H_2S detection.

The main aim of our work is the successful detection of H_2S trace amounts in the low ppb concentration range at room temperature. Therefore, we analyzed and compared resistive gas sensors based on pristine high quality ZnO NWs grown by high temperature chemical vapor deposition (CVD) with ZnO NWs after systematic surface modification with the noble metals Au and Pt. Resistive gas sensors based ZnO with nanoparticle layers ranging from 0–5 nm of catalyst thickness were investigated toward sensor response, signal-to-noise ratio, and limit of detection. We showed that Au/ZnO NW gas sensors are superior in comparison to gas sensors based on pristine ZnO NWs and Pt/ZnO NWs and allow for H_2S detection in synthetic air at room temperature with an estimated limit of detection of 7 ppb.

2. Materials and Methods

2.1. ZnO Nanowire Growth

ZnO NWs were grown by high temperature CVD using vapor liquid solid (VLS) growth [22] in a movable three-zone tube furnace with a horizontal quartz glass liner tube. The upstream side of the quartz glass liner tube had a gas inlet for argon (Ar, 99.998% purity, 190 sccm flow rate). The downstream side had a gas inlet for oxygen (O_2, 99.995% purity diluted in Ar down to 5%, 1.14 sccm flow rate) and was also connected to a vacuum pump. For the growth, 300 mg source material was used, which consisted of carbon powder and ZnO powder (99.99% purity) in the molar ratio 1:1. Substrate silicon (100) wafer pieces of 1 cm^2 total size with a 3 nm thick gold layer on top were used, the latter acting as a catalyst for the NW growth. The source material was placed upstream inside the three-zone furnace at a temperature of 1045 °C. The substrate was placed 25 cm downstream from the source material at a temperature of 1057 °C. The oxygen inlet was 1 cm upstream next to the substrate. Growth took place at stabilized tube pressure of 900 mbar. During the 60 min long growth process, evaporated ZnO was reduced to Zn vapor, which was transported by the argon carrier gas toward the oxygen inlet and substrate. Here the Zn re-oxidized to ZnO within the catalytic Au/Zn alloy droplets on the Si substrate surface. These droplets acted as nucleation sites for the ZnO NW growth. After successful growth, we obtained a dense nanowire forest of approximately 40 μm long and 100 nm thick ZnO NWs as shown in Figure 1a.

A detailed study about the ZnO NW growth process was reported in previous work by Li et al. and Huber et al. [23,24].

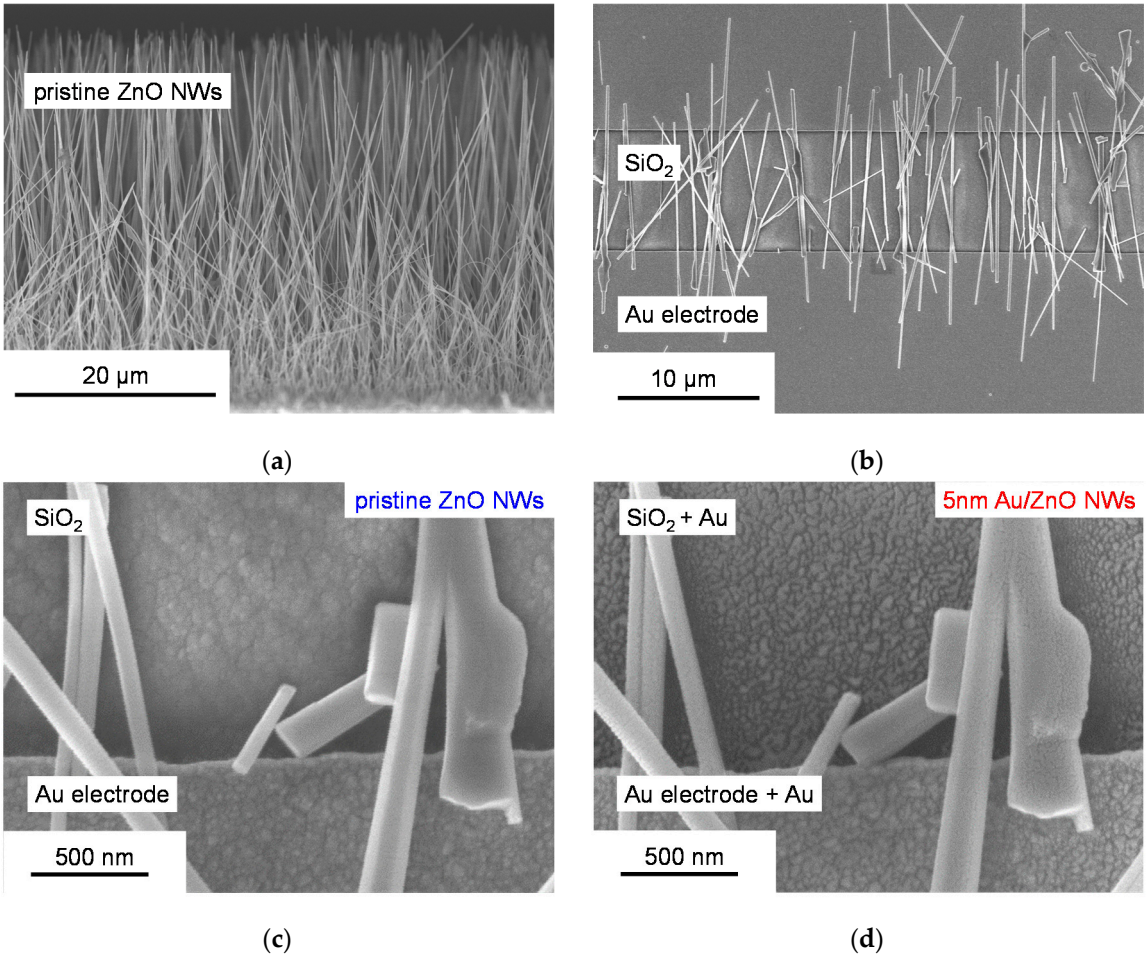

Figure 1. Scanning electron micrographs of (**a**) pristine ZnO NWs as grown on Si with Au catalyst and (**b**) after deposition via dielectrophoresis between two parallel Au contact pads on the sensor surface; (**c**,**d**) ZnO NWs before and after surface modification with 5 nm of Au by room temperature magnetron sputtering. The deposited metal catalyst forms a discontinuous nanoparticle layer.

2.2. Gas Sensor Fabrication and Metal Surface Modification of ZnO Nanowires

Sensors were fabricated from hundreds of ZnO NWs bridging the 5–10 µm gap between two Ti/Au contact stripes on a silicon substrate with 900 nm insulating SiO_2 on top (Figure 1b). In a first step, the ZnO NWs were harvested from the growth substrate with an ultra-sonification bath while being diluted in 1000 µL of isopropanol. In a second step, 40 µL of this solution was drop coated onto a single contact structure and aligned by dielectrophoresis [25]. For a reproducible and homogeneous surface modification of the ZnO NW sensors, Au and Pt were deposited by magnetron sputtering. Here, a Bal-Tec Med 020 high vacuum coating system was used. The investigated nanoparticle layer thicknesses ranged from 0–5 nm. A nanoparticle layer thickness higher than 5–7 nm leads to a shortcut, and hence prohibited sensing via the ZnO NWs [26]. The sputtering values for Au and Pt deposition at room temperature were 5×10^{-2} Pa base pressure and 7×10^{-3} Pa sputtering pressure, a sputtering power of 7 W, and a target size of 2″. After 90 s a uniform Au film of 5 nm could be achieved. During the sputtering process the film thickness was monitored via a quartz crystal microbalance placed next to the sensor samples. This microbalance was calibrated for Au and Pt magnetron sputtering by X-ray reflectometry (XRR) measurements using test samples. Figure 1c,d shows the sensor surface before and after surface modification with 5 nm Au nanoparticle layer thickness. During surface modification metal nanoparticle islands were formed and created a discontinuous film. A thicker nanoparticle catalyst loading will close the gaps between the islands and lead to a continuous and conducting layer, hence leading to the unwanted shortcut between the contact pads of the sensor.

2.3. Measurement Setup and Gas Sensor Evaluation

A schematic representation of our gas sensing setup is displayed in Figure 2a with the measurement chamber encircled in red. The chamber was a circular stainless steel gas compartment with a small total gas volume of 11 mL (Figure 2c) and room for two sensors, which could be measured simultaneously. The chamber was temperature stabilized by a water bath. General gas testing measurements were executed at a stable room temperature of (20 ± 1) °C in dynamic flux measurements under a gas flow of 42 sccm/min. The tested gas atmosphere was pre-mixed and diluted in a computer-controlled mixing stage consisting of several mass flow controllers and one pressure controller. Gases used in our measurements were 1 ppm of H_2S (98% purity) pre-diluted in nitrogen (N_2, 99.9999% purity), which could be diluted further with nitrogen (N_2, 99.9999% purity) or synthetic air (N_2, 99.9999% purity, with O_2, 99.995% purity, mixed in a N_2:O_2 ratio of 4:1), pure nitrogen (N_2, 99.9999% purity), and pure oxygen (O_2, 99.995% purity). Each selected atmosphere was tested in general 10 min long intervals, alternating between the testing gas atmosphere and a flushing gas atmosphere in a series of multiple detection cycles. For the electrical evaluation of the gas measurement response, we applied 1 V to every sensor (Figure 2b) and acquired the current flow I through the ZnO NWs over the time t with a combination of switchable low-noise transimpedance amplifiers and a 12-bit analog–digital converter (ADC). Data were recorded with an acquisition rate of $1/s$. As a result, an $I(t)$ trace was measured and further investigated by the estimatation of the reference current level I_0 (or quiescent current level) in a neutral flushing gas interval, which was acquired for each sensor by flushing the samples with pure N_2, O_2, or synthetic air for a minimum of 10 min before introducing the desired target gas to the sensor. Based on the reference current level, the response is defined as [27]:

$$R(\%) = \left(I_g - I_0\right)/I_0 \cdot 100, \quad (1)$$

where I_g is the measured current level through the ZnO NWs at the end of a target gas. The sensitivity is defined as the slope of the response ΔR over the detected target gas concentration Δc:

$$S = \frac{\Delta R}{\Delta c}, \quad (2)$$

which is needed in order to estimate the theoretical LOD value via the given definition [28]:

$$LOD = 3\frac{RMS}{S}, \quad (3)$$

where, RMS stands for the root mean square noise of the response R and is further used to estimate the signal-to-noise ratio:

$$SNR = \frac{RMS}{R}, \quad (4)$$

of our sensors.

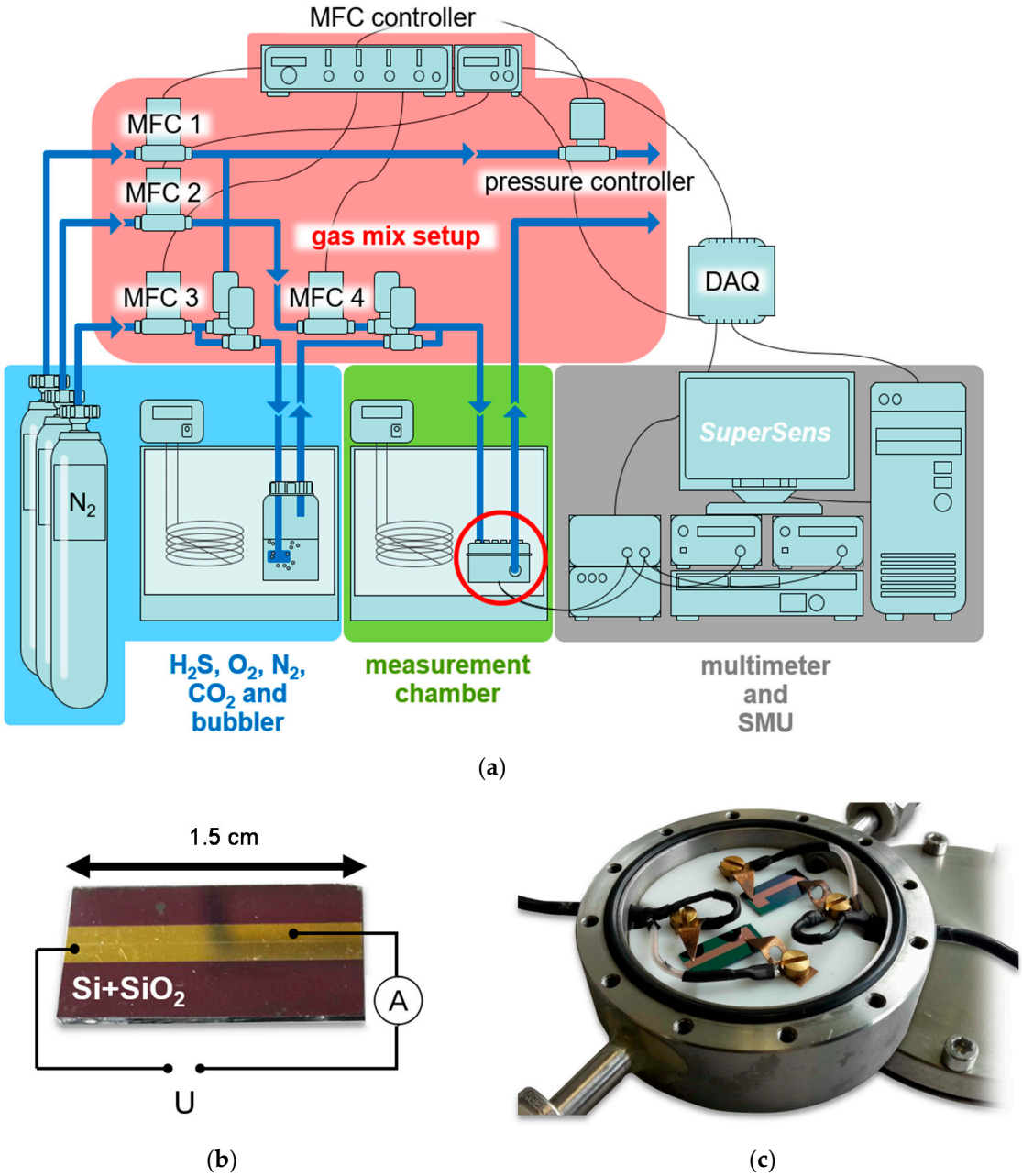

Figure 2. Schematic overview of core components of the measurement setup: (**a**) gas sensing setup with computer-controlled mixing stage, multiple high purity gases, temperature-stabilized measurement chamber encircled in red and data acquisition; (**b**) planar sensor with two 1.5 cm long parallel Au electrodes on Si with insulating SiO_2; (**c**) sealed stainless steel measurement chamber with a total gas compartment of 11 mL and two gas sensors mounted.

3. Results

3.1. Gas Sensing with Pristine, Au-Modified and Pt-Modified ZnO Nanowires

The main aim of this work is to achieve a first and detailed understanding of the effects of surface modification of ZnO NWs with metal catalysts, here especially Au and Pt, on gaseous H_2S detection. The detection of H_2S with sensors using initially pristine ZnO NWs was compared to H_2S detection results of the same sensors after metal catalyst deposition. In order to separate the role of both metal catalysts from the general sensing attributes of ZnO, the sensor characteristics, e.g., the response R towards 1 ppm of H_2S, sensitivity S and LOD, were evaluated and compared between samples with pristine and surface-modified ZnO NWs of the same CVD growth batch.

For the first measurement series two sensors loaded with pristine ZnO NWs from the same growth run, were fabricated. The $I(V)$-curves of both sensors are displayed in Figure 3 and showed a comparable current level of 7.2 µA and 8.9 µm at 1 V, respectively. After electrical comparison of both sensors, they were tested in a first gas sensing measurement. The surrounding atmosphere for both sensors was periodically switched between pure O_2 and 1 ppm of H_2S diluted in N_2, starting with O_2 as the flushing gas interval and H_2S diluted in N_2 as the target gas interval. The $R(t)$-data for sensor 1 and sensor 2 are shown in Figure 4a. The response of the ZnO NWs towards H_2S appears to be hardly visible and reaches $R = (20 \pm 15)\%$ for sensor 2 when considering the noise level. Since the SNR for both sensors with pristine ZnO NWs appeared was close to 2, and hence the noise was very high in comparison to the detection signal, an estimation of the response for both sensors was difficult.

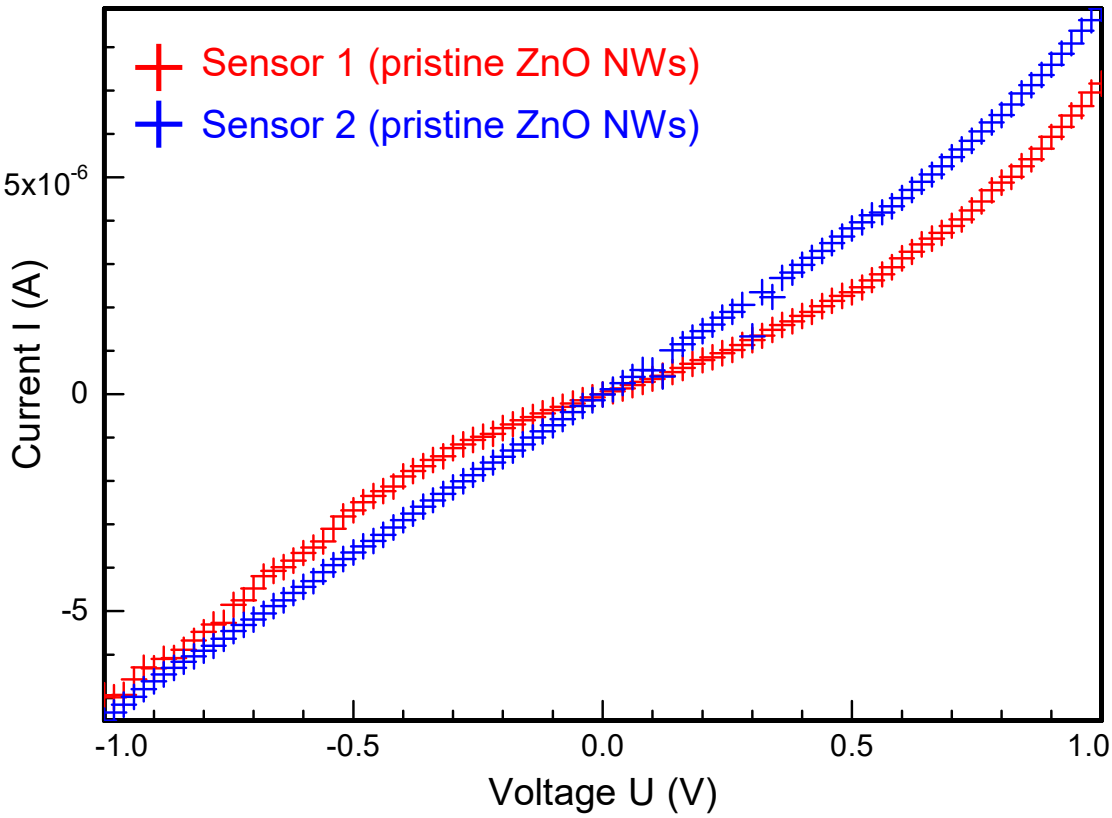

Figure 3. Nonlinear and symmetric $I(V)$-curve of two nominally identical sensors with pristine ZnO NWs fabricated from the same growth sample.

In the next step, 5 nm Au was deposited on sensor 2, and H_2S sensing measurements were performed with sensor 1 and sensor 2 again. In Figure 4b the $R(t)$-data for sensor 1 and sensor 2 after the modification of sensor 2 are displayed. The modified sensor 2 reached a response of $R = (5480 \pm 15)\%$ towards 1 ppm H_2S in the first detection cycle. As expected, the signal of sensor 1 stayed noisy with a response R below 100%. This tremendous increase of response toward 1 ppm of H_2S with Au-modified ZnO NWs in comparison to pristine ZnO NWs clearly demonstrated the beneficial effect of Au modification for H_2S detection with ZnO NWs. A closer look into the $R(t)$-data of sensor 2 after the modification revealed that the enhancement of the sensors response due to the Au catalyst seems to decrease over time. Therefore, the response in the second detection cycle in Figure 4b only reached $R = (3840 \pm 15)\%$. Continous testing of sensor 1 and sensor 2 for one week after modification revealed a strong decay of the sensors' response (Figure 4c,d). After one week of measurement the response of sensor 2 towards 1 ppm of H_2S decreased but also stabilized at $R = (25 \pm 5)\%$, with an improved SNR of 5 in comparison to the equivalent measurement of ZnO NWs

without modification. After one week of measurements no clear response could be acquired for the pristine ZnO NWs of sensor 1 due to the high noise level.

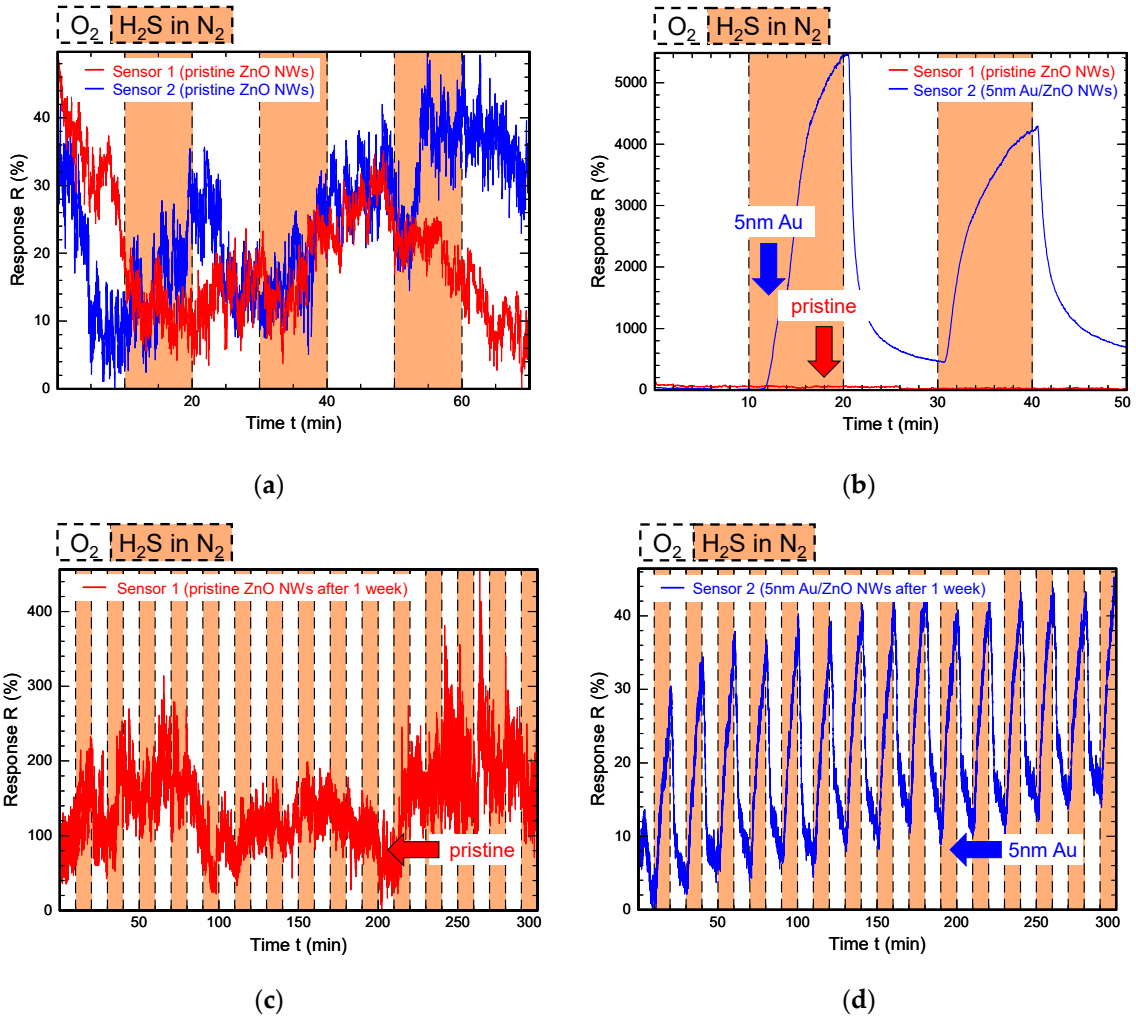

Figure 4. Comparison of H_2S detection results of pristine or Au surface-modified ZnO NWs. (**a**) $R(t)$-data of sensor 1 and sensor 2 before surface modification, reaching a response of $R = (20 \pm 15)\%$ towards 1 ppm target gas concentration; (**b**) after 5 nm Au deposition on sensor 2 the response towards 1 ppm H_2S is drastically increased to $R = (5480 \pm 15)\%$; (**c**) after 1 week of continuous measurement sensor 1 showed a high noise level and no clear response towards 1 ppm H_2S; (**d**) after 1 week only the surface-modified sensor 2 still responds towards H_2S. Due to ongoing contamination of the Au catalyst the enhanced response decreased to a stable value of $R = (25 \pm 5)\%$.

In the second measurement series surface modifications of ZnO NWs with Pt or Au were compared. Two sensors were fabricated from the same ZnO NW growth run by dropping 40 µL pristine ZnO NW solution onto two 1.5 cm long contact structures. After successful dielectrophoresis alignment sensor 1 was modified with 5 nm Au, and sensor 2 with 3 nm Pt. Any higher Pt loading would lead to a shortcut, as mentioned in Section 2.2, and hence was not considered for comparison. Both sensors were tested at room temperature in a total of 13 detection cycles by periodically switching between the flushing gas atmosphere of pure O_2 and the testing gas atmosphere of 1 ppm H_2S diluted in N_2. Figure 5a,b displays the measured $I(t)$-data of both sensors. Because of the visible upwards drift for both sensors, the corresponding responses for each detection cycle are displayed separately in Figure 5c. Comparing the $I(t)$-data of 5 nm Au/ZnO NWs with 3 nm Pt/ZnO NWs revealed a better SNR after Pt modification than after Au modification, which can be attributed to a unaffected noise level despite an increased reference current level. The response was enhanced for both sensors and reached a peak response of $R = (570 \pm 40)\%$ for sensor 1 with Au modification in

comparison to a peak response of $R = (40 \pm 1)\%$ for sensor 2 with Pt modification. A decrease in response toward 1 ppm H_2S with ongoing measurement cycles was observed for both sensors. For the Au-modified sensor the peak response decreased by a factor of 3 down to a stable response of $R = (190 \pm 40)\%$, whereas the already lower peak response of the Pt-modified sensor decreased by a factor of 13 down to a stable response of $R = (3 \pm 1)\%$. Both sensors, especially the Pt-modified ZnO NWs, showed an upwards drift of the reference current level. This was most likely caused by a catalytically assisted accumulation of H_2S on the ZnO NW surface in the testing gas interval, which led to a desorption reaction of O_2 in comparison to the less likely O_2 adsorption, which should take place in the flushing gas interval. This drift will be discussed in Section 4 in closer detail.

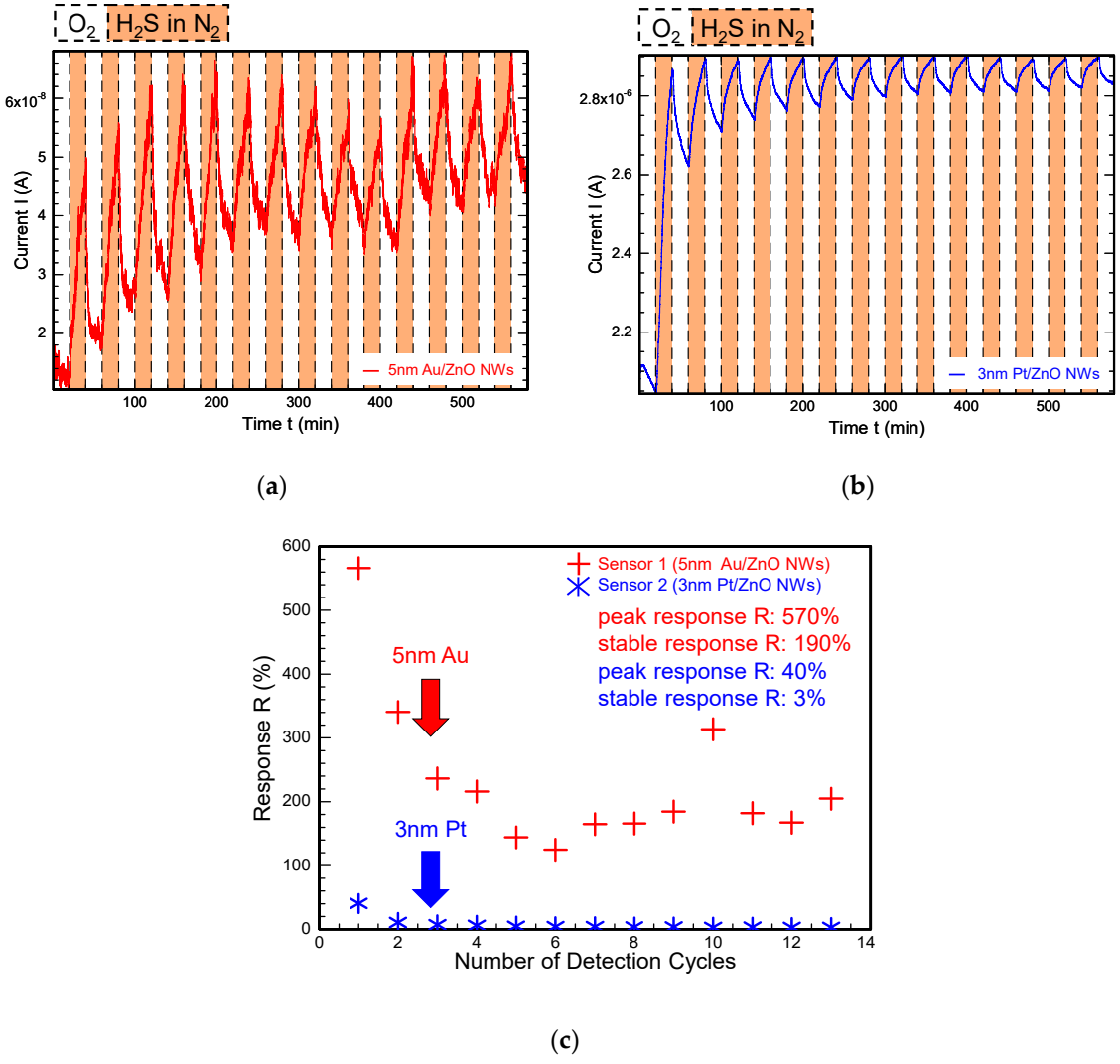

Figure 5. Comparison of H_2S detection results of Au and Pt surface-modified ZnO NWs. (**a**,**b**) $I(t)$-data of sensor 1 and sensor 2 after surface modification with 5 nm Au and 3 nm Pt towards 1 ppm H_2S, respectively; (**c**) equivalent response data for both sensors collected for 13 continuous measurement cycles. The response towards H_2S with Au-modified ZnO NWs appears to be superior with a peak response of $R = (570 \pm 40)\%$, in comparison to a peak response of $R = (40 \pm 1)\%$ with Pt-modified ZnO NWs. Both sensors show a continuously decreasing H_2S response due to a contamination of the metal catalyst caused by ongoing H_2S exposure.

Overall, our comparison of pristine, Au-modified and Pt-modified ZnO NWs demonstrated that Au is a reliable and more stable catalyst for H_2S detection with ZnO NWs than Pt.

3.2. Systematic Au Surface Modification of ZnO NWs

So far, we verified Au as a stable and promising catalyst candidate for gaseous H_2S detection with ZnO NWs. For a more detailed understanding of the catalytical effects of Au modification on the ZnO NW surface further investigation regarding a dependance between response enhancement and Au nanoparticle layer thickness and a closer look into the stability of the Au modification over time was done.

Therefore, a new sensor with initially pristine NWs was manufactured and tested for 1 ppm H_2S detection in 10 min long testing gas intervals. After the first recorded gas measurement results, the sensor was modified with a 1 nm thick Au nanoparticle layer and then tested for 1 ppm H_2S detection again. This increase of Au loading in steps of 1 nm on a single sensor and the corresponding evaluation was continued until the final Au nanoparticle layer thickness of 5 nm was deposited. Hence, $R(t)$-data for 1 ppm H_2S detection with pristine ZnO NWs and ZnO NWs with 1 nm, 2 nm, 3 nm, 4 nm and 5 nm Au catalyst loading on a single sensor were acquired and are displayed in Figure 6 and Table 1. The total measurement duration took 4 days.

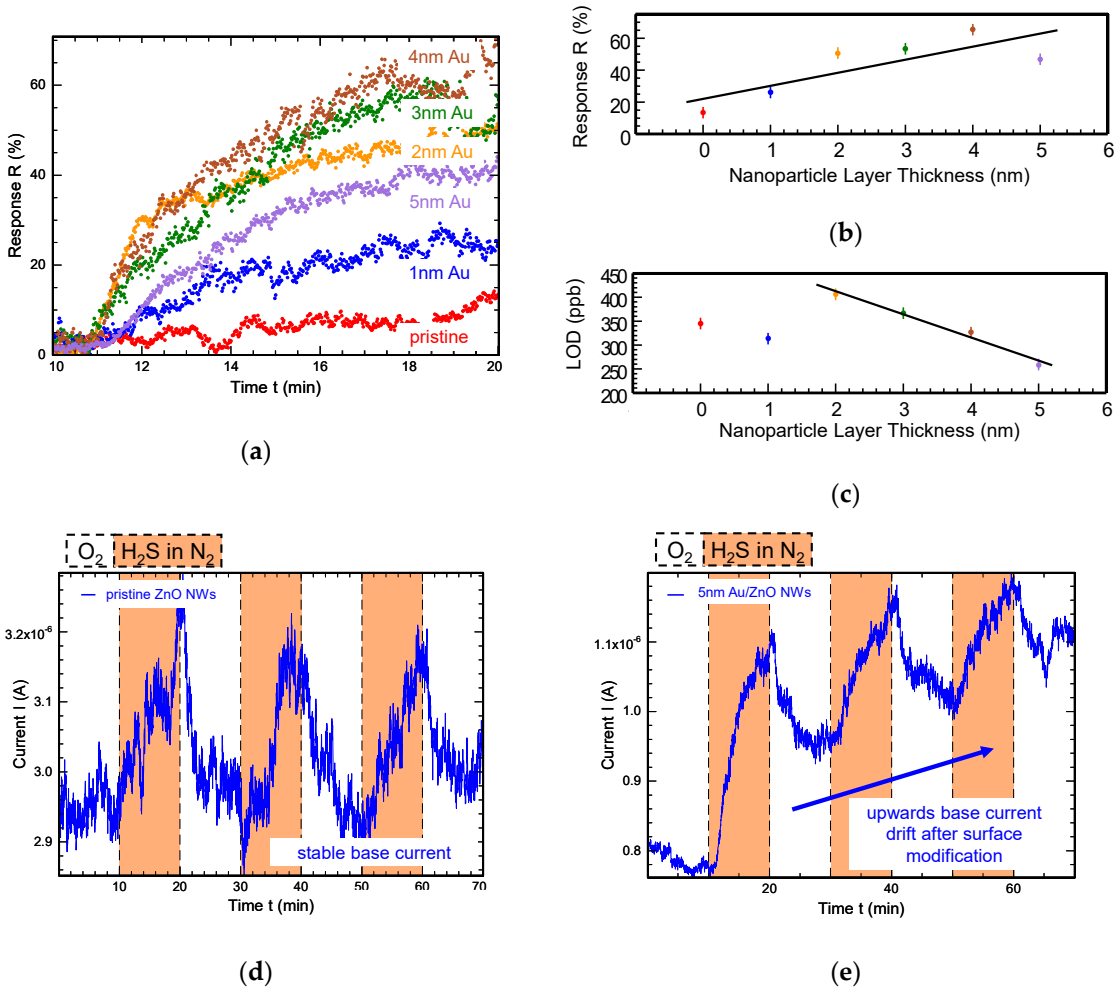

Figure 6. H_2S detection results for stepwise Au-modified ZnO NWs: (**a**) $R(t)$-data towards 1ppm H_2S for pristine ZnO NWs in the first target gas interval, and ZnO NWs modified by 1 nm, 2 nm, 3 nm, 4 nm, and 5 nm for the same sensor. (**b**,**c**) With increasing Au catalyst loading the response increased from initial $R = (13 \pm 5)\%$ with pristine ZnO NWs to up to $R = (65 \pm 5)\%$ with 4 nm Au/ZnO NWs. The LOD decreased with stepwise Au modification in an apparently linear tendency, which is displayed as a black curve. (**d**,**e**) Direct comparison of raw $I(t)$-data before and after surface modification of sensor 1. After the modification with Au, sensors showed an upwards base current drift as a result of favored detection of H_2S in comparison to O_2 adsorption.

The sensor with pristine ZnO NWs reached a response of $R = (13 \pm 5)\%$ for 1 ppm H_2S. This response continuously increased until the sensor reached a response of $R = (65 \pm 5)\%$ towards 1 ppm H_2S with 4 nm Au/ZnO NWs. For 5 nm Au catalyst loading the response decreased. The RMS for the measurements appeared to be independent from the Au nanoparticle layer thickness. As displayed in Figure 6b, the response towards 1 ppm H_2S increased with a thicker Au catalyst layer and the LOD decreased from (405 ± 40) ppb down to (259 ± 40) ppb (Figure 6c) with a continuously improved initial $SNR = 9$ with pristine ZnO NWs to $SNR = 12$ with 5 nm Au/ZnO loading.

This measurement series revealed a continuous improvement of several gas sensor characteristics like response R, SNR and LOD with increasing catalyst loading. It is very likely that a decreasing sensor response in spite of an increasing catalyst layer thickness was attributed to the decay of the catalyst itself during 4 days of continuous measurements. This decay was already observed in Section 3.1 and appeared after a first introduction of H_2S toward the sensors. The response toward H_2S with the 5 nm Au/ZnO NWs in this measurement series appeared to be lower than in the previous results, which were discussed in Section 3.1. This was also very much a consequence of the ongoing decay of the catalyst.

Figure 6d and Figure 6e display a direct comparison of the raw $I(t)$-data of sensor 1 towards the detection of 1 ppm H_2S before and after the completed surface modification of the ZnO NWs. It is clearly visible how the base current level showed drifting behavior only after the nanowire modification, which will be discussed in Section 4 in more detail.

Table 1. H_2S response results and LOD for stepwise Au-modified ZnO NWs.

Sensor	Response R (%)	LOD (ppb)
pristine ZnO NWs	13 ± 5	345 ± 40
1 nm Au/ZnO NWs	26 ± 5	313 ± 40
2 nm Au/ZnO NWs	51 ± 5	405 ± 40
3 nm Au/ZnO NWs	53 ± 5	366 ± 40
4 nm Au/ZnO NWs	65 ± 5	326 ± 40
5 nm Au/ZnO NWs	47 ± 5	259 ± 40

3.3. LOD Toward H_2S Detection in Synthetic Air with Pristine and Surface-Modified ZnO NWs

So far, we have investigated the detection of H_2S diluted in N_2 to low ppm concentrations. For a first attempt on medical breath analysis with pristine and surface-modified ZnO NWs an investigation of H_2S detection in the ppb range is of great interest. In order to model a first basic breath sample, H_2S needs to be diluted in dry synthetic air.

Therefore, two more sensors from the same ZnO NWs growth sample were processed, and their gas sensing abilities were tested toward low ppb-concentrations of H_2S diluted in dry synthetic air. Sensor 1 was fabricated from pristine ZnO NWs, and sensor 2 used nominally identical pristine ZnO NWs with additional surface modification of a 5 nm Au layer. Both sensors were tested in sensing cycles of 20 min long flushing gas intervals and testing gas intervals. The flushing gas was dry synthetic air, and the testing gas was 60–180 ppb of H_2S diluted in dry synthetic air. Additional 30 min intervals of pure O_2 in between different H_2S concentrations made sure that both sensors experienced different concentrations at comparable starting conditions.

The results of this measurement are displayed in Figure 7. Figure 7a shows the $R(t)$-data for both sensors. Sensor 1 with pristine ZnO NWs showed no response toward 60 ppb, 120 ppb, or 180 ppb of H_2S diluted in dry synthetic air. The surface-modified sensor 2 showed a clear response of $R = (250 \pm 60)\%$ towards 60 ppb of H_2S. This response increased to $R = (780 \pm 60)\%$ for the detection of 180 ppb of H_2S. As displayed in Figure 7b, the detection data of sensor 2 showed a clear linear dependence between response R and the detected concentration c. With a sensitivity of $S = (4400 \pm 300)\ \mathrm{ppm}^{-1}$ and a RMS of 10, this led to a theoretically estimated LOD of (7 ± 5) ppb for the detection of H_2S diluted in dry synthetic air at room temperature. This experimentally and

theoretically acquired LOD result for surface-modified ZnO NWs in comparison to pristine ZnO NWs highlighted the necessity and great potential of metal catalysts for H_2S detection with ZnO NWs. The selective detection of the resistive gas H_2S in the low ppb concentration range side by side with the strongly oxidative O_2 was the cause of the strong chemical affinity between Au and S and is discussed in Section 4.

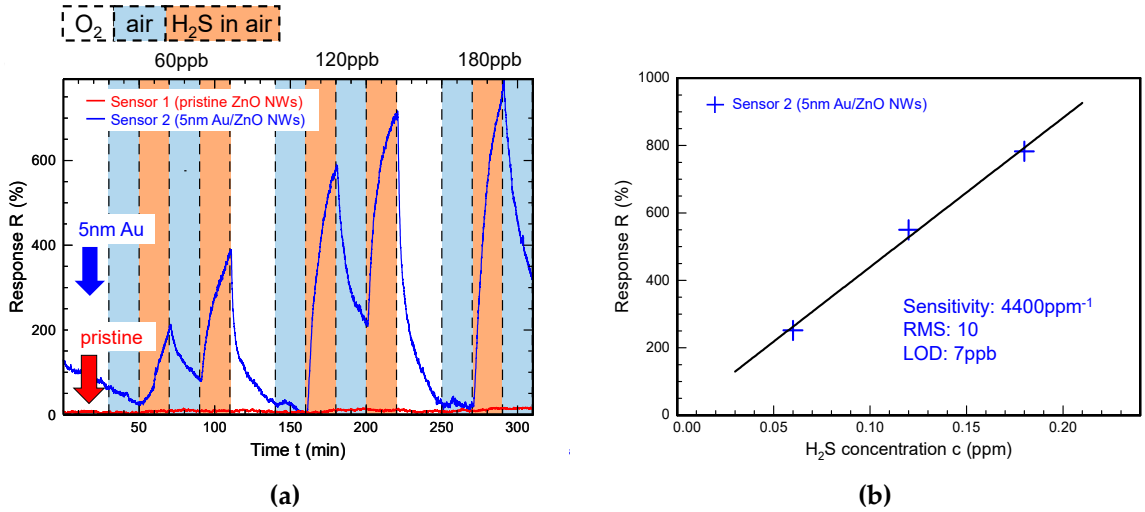

Figure 7. Detection results for H_2S diluted in synthetic air with pristine and Au-modified ZnO NWs: (**a**) Pristine ZnO NWs showed no reaction toward 60 ppb of H_2S diluted in air, while Au-modified ZnO NWs enabled the detection of H_2S in the low ppb range. (**b**) A theoretical estimation of the sensor sensitivity towards H_2S in diluted air led to a LOD of 7 ppb.

4. Discussion

The gas response mechanism of ZnO NWs is explained by adsorption and desorption reactions of reductive and oxidative gas molecules on a metal oxide surface. Nominally undoped ZnO typically is an n-type semiconductor due to surface and defect states such as oxygen vacancies. These additional states lead to the formation of a permanent non-conducting depletion layer at the ZnO NW surface and a remaining n-type conductive nanowire core.

When ZnO gets exposed to an oxidizing gas such as oxygen, these molecules ionosorb to active adsorption sites on the nanowire surface by trapping electrons from the n-type conducting core to themselves, as shown in Figure 8a. This leads to an agglomeration of adsorbed anionic oxygen species, representing an additional negative charge, causing an upwards bending of the ZnO band structure at the nanowire, reducing the diameter of conductive core. Thus, the resistance of the ZnO NWs increases and the current through the wires drops. At room temperature the adsorption process of the flushing gas O_2 can be described as [29]:

$$O_2 \rightarrow O_{2(ads)}, \quad (5)$$

$$O_2 + e^- \rightarrow O^-_{2(ads)}. \quad (6)$$

If, in turn, a reducing gas, in our case the target gas H_2S, is brought in contact with the ZnO NWs, it reacts with the previously adsorbed oxygen species, which leads to a desorption of the latter [30,31]:

$$2H_2S_{(g)} + 3O^-_{2(ads)} \rightarrow 2SO_{2(g)} + 2H_2O_{(g)} + 3e^-. \quad (7)$$

The freed electrons are released back to the conducting nanowire core, and the surface band bending is reduced, i.e., the depletion region becomes thinner and the conducting core becomes wider, resulting in a higher current. This adsorption and desorption reaction of oxidative and reductive gas is observed commonly for metal oxides, and specifically for pristine ZnO NWs.

If a metal catalyst such as Au or Pt is introduced to a metal oxide surface, a series of possible effects are mentioned in literature that will have a strong impact on the gas-response mechanism. A commonly reported effect for surface modification of metal oxides with Au and Pt is the formation of multiple nano-Schottky barriers at the contact region between the metal oxide and the metal catalyst (Figure 8b) [32]. The work function of Au and Pt [33] is larger than that of ZnO [34], which leads to a transfer of electrons from the nanowire core to the noble metal islands on the surface. These additional "nano-depletion regions" will be modulated by ongoing oxygen adsorption and desorption, leading to a greatly enhanced resistance and current change within the ZnO NWs and, hence, an enlarged response. This effect was easily confirmed by our measurements in the case of Au.

Another beneficial effect for gas detection with metal-modified metal oxides, especially Au-modified ZnO NWs, is the catalytically activated dissociation of H_2S molecules on Au nanoparticle islands [35]. Because of a chemical affinity between Au and S, Au islands are active agglomeration sites for H_2S molecules (Figure 8c). This agglomeration leads to a quantitively increased interaction between H_2S molecules and previously adsorbed O_2 molecules, which is supported by the improved R and LOD of our Au-modified sensors.

A similar effect is expected for the catalytic dissociation of oxygen at Au and Pt nanoparticle island [36,37]:

$$O_2 \rightarrow 2O(Au), \tag{8}$$

$$O(Au) + 2e^- \rightarrow O^{2-}{}_{(ads)}, \tag{9}$$

and [38]:

$$O_2 \rightarrow 2O(Pt), \tag{10}$$

$$O(Pt) + 2e^- \rightarrow O^{2-}{}_{(ads)}. \tag{11}$$

This catalytic ionization of O_2 should greatly enhance the adsorption reaction of O_2 and should result in a significantly decreased reference current level or a highly increased absorption rate for oxygen in our flushing gas intervals. However, our data do not support an enhanced dissociation of oxygen after surface modification of initially pristine ZnO NWs. A visible reference current drift after surface modification with said metal catalysts indicates a favoured H_2S dissociation instead of an oxygen dissociation. This is further confirmed by the successful detection of H_2S concentrations in the low ppb range in synthetic air. Here, 60 ppb of H_2S can be detected in the presence of 15% of highly oxidative O_2 (as shown in Figure 7a,b).

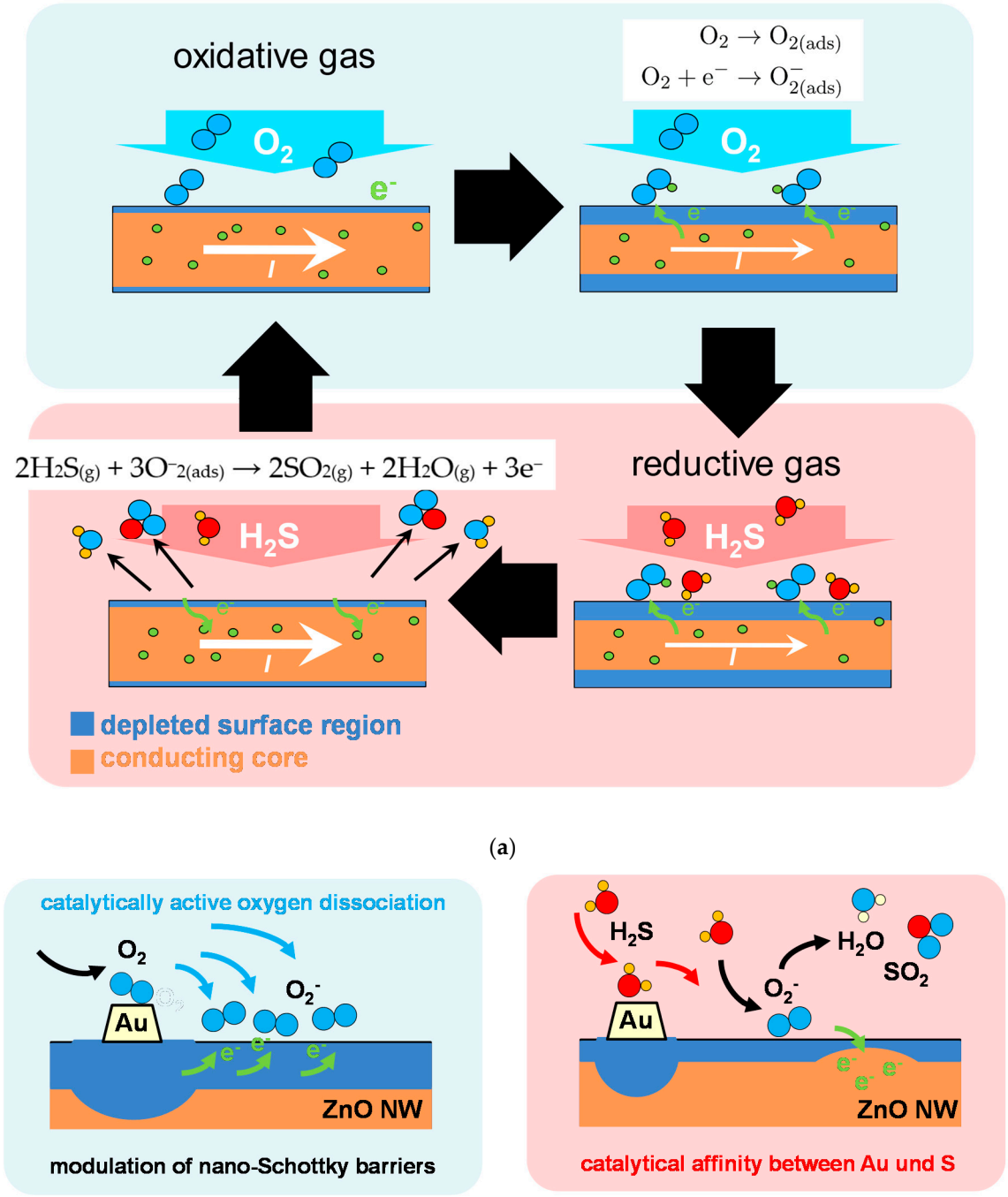

Figure 8. Gas-response mechanism of (**a**) pristine ZnO NWs; (**b**) Au- and Pt-modified ZnO NWs, as well as (**c**) the catalytic affinity between Au-modified ZnO NWs and S. Multiple additional nano-depletion regions on metal-modified ZnO NWs lead to an enhanced response of the gas sensors. The affinity between Au and S leads to a selective detection of H_2S with Au-modified ZnO NWs and enables H_2S detection in the low ppb concentration range.

While the catalytic dissociation of H_2S due to the Au surface modification led to a tremendous enhancement of the sensitivity of ZnO NWs, the strong affinity between Au and S may also be the reason for an ongoing and irreversible contamination of the catalyst as well. The strong chemical affinity between Au and S presumably led to a reactive interaction between both elements [32,39,40]:

$$H_2S_{(g)} + Au_{(s)} \rightarrow AuS_{(s)} + H_{2(g)}. \quad (12)$$

H_2S agglomerates at the Au islands and reacts to Au–SH and Au–S type species, which results in a sulfurization of the Au catalyst over time [32]. Continuous exposure to H_2S decreases the catalytic efficiency of Au-modified ZnO NWs. This behaviour was observed for each sensor sample after Au surface modification and needs further investigation in order to use Au/ZnO as a reliable sensing material for H_2S detection in the low ppb concentration range.

5. Conclusions

H_2S gas detection in the low ppb concentration range was successfully performed with pristine, Au-modified and Pt-modified ZnO NWs. The nanowires were grown by high temperature CVD on Si (100) with a thin Au layer on top acting as growth catalyst. The as-grown ZnO NWs were deposited via dielectrophoresis and functionalized with Au and Pt using magnetron sputtering at room temperature. Systematic comparison of H_2S detection with pristine and modified nanowires of the same nanowire growth process was performed, including Pt catalyst loadings of 3 nm and Au catalyst loadings of 1 nm, 2 nm, 3 nm, 4 nm and 5 nm. Surface modification with Au led to a consistent enhancement of the gas sensing properties such as response R, SNR, and LOD. While this was expected from literature for both Au and Pt modification, our measurements could only confirm the catalytically enhanced detection of H_2S with Au surface-modified ZnO NWs. The so far investigated modification method led to a large enhancement of the sensitivity; however, this initial improvement also decreased with ongoing H_2S exposure due to a degradation of the applied metal catalysts. This was most likely caused by a sulfurization process of the catalyst, which could be expected because of the strong chemical interaction between sulfur and Au. On the other hand, the same chemical interaction allowed for the detection of extremely low experimentally and theoretically estimated $LODs$ of 60 ppb and 7 ppb of H_2S diluted in synthetic air at room temperature, and hence highlights Au/ZnO NWs as a very potent sensing material for biomarker detection in the low ppb concentration range.

Author Contributions: Conceptualization, A.K.; methodology, A.K., F.H., U.H. and K.T.; software, K.T.; validation, A.K., E.T.C., F.H., U.H. and K.T.; formal analysis, A.K. and E.T.C.; resources, U.H. and K.T.; data curation, A.K. and E.T.C.; writing—original draft preparation, A.K.; writing—review and editing, A.K., U.H. and K.T.; visualization, A.K.; supervision, U.H. and K.T.; project administration, U.H. and K.T. All authors have read and agreed to the published version of the manuscript.

Funding: We thank the DFG-Deutsche Forschungsgemeinschaft for funding this project under contract number 398819137.

Acknowledgments: The authors thank H. Schieferdecker for the dedicated technical support in the measurement setup.

References

1. Wang, P.; Zhang, G.; Wondimu, T.; Ross, R.; Wang, R. Hydrogen sulfide and asthma. *Exp. Physiol.* **2011**, *96*, 847–852, doi:10.1113/expphysiol.2011.057448.
2. Szabó, C. Hydrogen sulphide and its therapeutic potential. *Nat. Rev. Drug. Discov.* **2007**, *6*, 917–935, doi:10.1038/nrd2425.
3. D'Amico, A.; Pennazza, G.; Santonico, M.; Martinelli, E.; Roscioni, C.; Galluccio, G.; Paolesse, R.; Di Natale, C. An investigation on electronic nose diagnosis of lung cancer. *Lung Cancer* **2010**, *68*, 170–176, doi:10.1016/j.lungcan.2009.11.003.
4. Millonig, G.; Praun, S.; Netzer, M. Non-invasive diagnosis of liver diseases by breath analysis using an optimized ion-molecule reaction-mass spectrometry approach: A pilot study. *Biomarkers* **2010**, *15*, 297–306, doi:10.3109/13547501003624512.
5. Zhang, J.; Wang, X.; Chen, Y.; Yao, W. Correlation between levels of exhaled hydrogen sulfide and airway inflammatory phenotype in patients with chronic persistent asthma. *Respirology* **2014**, *19*, 1165–1169, doi:10.1111/resp.12372.
6. Wondimu, T.; Wang, R.; Ross, B. Hydrogen sulphide in human nasal air quantified using thermal desorption and selected ion flow tube mass spectrometry. *J. Breath Res.* **2014**, *8*, 036002, doi:10.1088/1752-7155/8/3/036002.

7. Zampolli, S.; Elmi, I.; Mancarella, F.; Betti, P.; Dalcanale, E.; Cardinali, G.C.; Severi, M. Real-time monitoring of sub-ppb concentrations of aromatic volatiles with a MEMS-enabled miniaturized gas-chromatograph. *Sens. Actuators B: Chem.* **2009**, *141*, 322–328, doi:10.1016/j.snb.2009.06.021.
8. Petruci, J.; Cardoso, A.A.; Wilk, A.; Kokoric, V.; Mizaikoff, B. iCONVERT: An Integrated Device for the UV-Assisted Determination of H2S via Mid-Infrared Gas Sensors. *Anal. Chem.* **2015**, *87*, 9580–9583, doi:10.1021/acs.analchem.5b02731.
9. Petruci, J.; Cardoso, A.A.; Wilk, A.; Mizaikoff, B. Online Analysis of H_2S and SO_2 via Advanced Mid-Infrared Gas Sensors. *Anal. Chem.* **2015**, *87*, 9605–9611, doi:10.1021/acs.analchem.5b02730.
10. Moon, H.G.; Jung, Y.; Han, S.D.; Shim, Y.; Shin, B.; Lee, T.; Kim, J.; Lee, S.; Jun, S.C.; Park, H.; et al. Chemiresistive Electronic Nose toward Detection of Biomarkers in Exhaled Breath. *ACS Appl. Mater. Interfaces* **2016**, *8*, 20969–20976, doi:10.1021/acsami.6b03256.
11. Ionescu, R.; Hoel, A.; Granqvist, C.G.; Llobet, E.; Heszler, P. Low-level detection of ethanol and H_2S with temperature-modulated WO_3 nanoparticle gas sensors. *Sens. Actuators B: Chem.* **2005**, *104*, 132–139, doi:10.1016/j.snb.2004.05.015.
12. Zhang, D.; Wu, J.; Cao, Y. Ultrasensitive H_2S gas detection at room temperature based on copper oxide/molybdenum disulfide nanocomposite with synergistic effect. *Sens. Actuators B: Chem.* **2019**, *287*, 346–355, doi:10.1016/j.snb.2019.02.008.
13. Choi, S.-J.; Jang, B.-H.; Lee, S.-J.; Min, B.K.; Rothschild, A.; Kim, I.-D. Selective Detection of Acetone and Hydrogen Sulfide for the Diagnosis of Diabetes and Halitosis Using SnO_2 Nanofibers Functionalized with Reduced Graphene Oxide Nanosheets. *ACS Appl. Mater. Interfaces* **2014**, *6*, 2588–2597, doi:10.1021/am405088q.
14. Yin, L.; Chen, D.; Feng, M.; Ge, L.; Yang, D.; Song, Z.; Fan, B.; Zhang, R.; Shao, G. Hierarchical Fe_2O_3@WO_3 nanostructures with ultrahigh specific surface areas: Microwave-assisted synthesis and enhanced H_2S-sensing performance. *RSC Adv.* **2015**, *5*, 328–337, doi:10.1039/C4RA10500A.
15. Deng, J.; Fu, Q.; Luo, W.; Tong, X.; Xiong, J.; Hu, Y.; Zheng, Z. Enhanced H_2S gas sensing properties of undoped ZnO nanocrystalline films from QDs by low-temperature processing. *Sens. Actuators B: Chem.* **2016**, *224*, 153–158, doi:10.1016/j.snb.2015.10.022.
16. Wu, Z.; Li, Z.; Li, H.; Sun, M.; Han, Sh.; Cai, C.; Shen, W.; Fu, Y. Ultrafast Response/Recovery and High Selectivity of the H_2S Gas Sensor Based on α-Fe_2O_3 Nano-Ellipsoids from One-Step Hydrothermal Synthesis. *ACS Appl. Mater. Interfaces* **2019**, *11*, 12761–12769, doi:10.1021/acsami.8b22517.
17. Wang, C.; Chu, X.; Wu, M. Detection of H_2S down to ppb levels at room temperature using sensors based on ZnO nanorods. *Sens. Actuators B: Chem* **2006**, *113*, 320–323, doi:10.1016/j.snb.2005.03.011.
18. Miller, D.R.; Akbar, S.A.; Morris, P.A. Nanoscale metal oxide-based heterojunctions for gas sensing: A review. *Sens. Actuators B: Chem.* **2014**, *204*, 250–272, doi:10.1016/j.snb.2014.07.074.
19. Tai, H.; Wang, S.; Duan, Z.; Jiang, Y. Evolution of breath analysis based on humidity and gas sensors: Potential and challenges. *Sens. Actuators B: Chem.* **2020**, *318*, 128104, doi:10.1016/j.snb.2020.128104.
20. Sharma, P.K.; Ramgir, N.S.; Goyal, C.P.; Datta, N.; Srivastava, S.; Kaur, M.; Debnath, A.K.; Aswal, D.K.; Vijay, Y.K.; Gupta, S.K. Effect of sensitizers on H_2S sensing properties of ZnO nanowires. In Proceedings of the International Conference on Advanced Nanomaterials & Emerging Engineering Technologies, Sathyabama University, 600119 Chennai, India, 25 July 2013; pp. 215–217, doi:10.1109/ICANMEET.2013.6609280.
21. Zhou, X.; Lin, X.; Yang, S.; Zhu, S.; Chen, X.; Dong, B.; Bai, X.; Wen, X.; Geyu, L.; Song, H. Highly dispersed Metal–Organic-Framework-Derived Pt nanoparticles on three-dimensional macroporous ZnO for trace-level H_2S sensing. *Sens. Actuators B: Chem.* **2020**, *309*, 127802, doi:10.1016/j.snb.2020.127802.
22. Wagner, R.S.; Ellis, W.C. Vapor-liquid-solid mechanism of single crystal growth. *Appl. Phys. Lett.* **1964**, *4*, 89–90, doi:10.1063/1.1753975.
23. Li, Y.; Feneberg, M.; Reiser, A.; Schirra, M.; Enchelmaier, R.; Ladenburger, A.; Langlois, A.; Sauer, R.; Thonke, K. Au-catalyzed growth processes and luminescence properties of ZnO nanopillars on Si. *J. Appl. Phys.* **2006**, *99*, 054307, doi:10.1063/1.2178395.
24. Huber, F.; Riegert, S.; Madel, M.; Thonke, K. H_2S sensing in the ppb regime with zinc oxide nanowires. *Sens. Actuators B: Chem* **2017**, *239*, 358–363, doi:10.1016/j.snb.2016.08.023.
25. Pohl, H.A. *Dielectrophoresis: The Behavior of Neutral Matter in Nonuniform Electric Field*; Cambridge University Press: New York, NY, USA, 1978.

26. Siegel, J.; Lyutakov, O.; Rybka, V.; Kolská, Z.; Svorčík, V. Properties of gold nanostructures sputtered on glass. *Nanoscale Res Lett.* **2011**, *6*, 96, doi:10.1186/1556-276X-6-96.
27. Kumar, R.; Al-Dossary, O.; Kumar, G.; Umar, A. Zinc Oxide Nanostructures for NO_2 Gas–Sensor Applications: A Review. *Nano-Micro Lett.* **2015**, *7*, 97–120, doi:10.1007/s40820-014-0023-3.
28. Wu, J.; Wu, Z.; Ding, H.; Yang, X.; Wei, Y.; Xiao, M.; Yang, Z.; Wang, X. Three-Dimensional-Structured Boron- and Nitrogen-Doped Graphene Hydrogel Enabling High-Sensitivity NO_2 Detection at Room Temperature. *ACS Sens.* **2019**, *4*, 1889–1898, doi:10.1021/acssensors.9b00769.
29. Barsan, N.; Weimar, U. Conduction model of metal oxide gas sensors. *J. Electroceramics* **2001**, *7*, 143–167.
30. Xu, J.; Wang, X.; Shen, J. Hydrothermal synthesis of In_2O_3 for detecting H_2S in air. *Sens. Actuators B: Chem.* **2006**, *115*, 642–646, doi:10.1016/j.snb.2005.10.038.
31. Kim, J.; Yong, K. Mechanism study of ZnO nanorod-bundle sensors for H_2S gas sensing. *J. Phys. Chem. C* **2011**, *115*, 7218–7224, doi:10.1021/jp110129f.
32. Choi, M.S.; Mirzaei, A.; Bang, J.H.; Oum, W.; Jung Kwon, Y.; Kim, J.-H.; Choi, S.-W.; Kim, S.S.; Kim, H.W. Selective H_2S-sensing performance of Si nanowires through the formation of ZnO shells with Au functionalization. *Sens. Actuators B: Chem.* **2019**, *289*, 1–14, doi:10.1016/j.snb.2019.03.047.
33. Michaelson, H.B. The work function of the elements and its periodicity. *J. Appl. Phys.* **1977**, *48*, 4729–4733, doi:10.1063/1.323539.
34. Choi, S.W.; Katoch, A.; Sun, G.J.; Kim, S.S. Synthesis and gas sensing performance of ZnO-SnO_2 nanofiber-nanowire stem-branch heterostructure. *Sens. Actuators B: Chem.* **2013**, *181*, 787–794, doi:10.1016/j.snb.2013.02.010.
35. Geng, J.; Thomas, M.D.R.; Shephard, D.S.; Johnson, B.F.G. Suppressed electron hopping in a Au nanoparticle/H_2S system: Development towards a H_2S nanosensor. *Chem. Commun* **2005**, *14*, 1895–1897, doi:10.1039/B418559E.
36. Rai, P.; Kim, Y.S.; Song, H.M.; Song, M.K.; Yu, Y.T. The role of gold catalyst on the sensing behavior of ZnO nanorods for CO and NO_2 gases. *Sens. Actuators B: Chem.* **2012**, *165*, 133–142. doi:10.1016/j.snb.2012.02.030.
37. Li, X.; Zhou, X.; Guo, H.; Wang, C.; Liu, J.; Sun, P.; Liu, F.; Lu, G. Design of Au@ZnO Yolk–Shell Nanospheres with Enhanced Gas Sensing Properties. *ACS Appl. Mater. Interfaces* **2014**, *6*, 18661–18667, doi:10.1021/am5057322.
38. Saito, S.; Miyayama, M.; Koumoto, K.; Yanagida, H. Gas Sensing Characteristics of Porous ZnO and Pt/ZnO Ceramics. *J. Am. Ceram. Soc.* **1985**, *68*, 40–43, doi:10.1111/j.1151-2916.1985.tb15248.x.
39. Balouria, V.; Ramgir, N.S.; Singh, A.; Debnath, A.K.; Mahajan, A.; Bedi, R.K.; Aswal, D.K.; Gupta, S.K. Enhanced H_2S sensing characteristics of Au modified Fe_2O_3 thin films. *Sens. Actuators B: Chem.* **2015**, *219*, 125–132, doi:10.1016/j.snb.2015.04.113.
40. Rai, P.; Yoon, J.W.; Jeong, H.M.; Hwang, S.J.; Kwak, C.H.; Lee, J.H. Design of highly sensitive and selective Au@NiO yolk–shell nanoreactors for gas sensor applications. *Nanoscale* **2014**, *6*, 8292–8299, doi:10.1039/C4NR01906G.